Nonlinear dynamics of two-dimensional convection in a vertically stratified slot with and without gravity modulation

By C. I. CHRISTOV† AND G. M. HOMSY

Department of Chemical Engineering Stanford University, Stanford, CA 94305, USA

The convective flow in a vertical slot with differentially heated walls and vertical temperature gradient is considered for very large Rayleigh numbers. Gravity is taken to be vertical and to consist of both a mean and a harmonic modulation ('jitter') at a given frequency and amplitude. The time-dependent Boussinesq equations governing the two-dimensional convection are solved numerically. To this end an economic operator-splitting scheme is devised combined with internal iterations within a given time step. The approximation of the nonlinear terms is conservative and no scheme viscosity is present in the approximation. The flow is investigated for a range of Prandtl numbers from $Pr = 1000$ when fluid inertia is insignificant and only thermal inertia plays a role to $Pr = 0.73$ when both are significant and of the same order. The flow is governed by several parameters. In the absence of jitter, these are the Prandtl number, Pr, the Rayleigh number, Ra, and the dimensionless critical stratification, τ_B. Simulations are reported for $Pr = 10^3$ and a range of τ_B and Ra, with emphasis on mode selection and finite-amplitude states. The presence of jitter adds two more parameters, i.e. the dimensionless jitter amplitude ϵ and frequency ω, rendering the flow susceptible to new modes of parametric instability at a critical amplitude ϵ_c. Stability maps of ϵ_c vs. ω are given for a range of ω. Finally we investigate the response of the system to jitter near the neutral curves of the various instability modes.

1. Introduction

Figure 1 gives a schematic of the stratified slot in which a Boussinesq fluid is held between two vertical plates. The slot width is L^* and the height of the domain, H^*. The driving force for the convection is the combination of an imposed temperature gradient and the buoyancy of the fluid. The wall temperatures are vertically stratified, but held at a fixed lateral difference from one another. The relevant boundary conditions on the horizontal boundaries are discussed below. As is well-know, the presence of vertical stratification admits a parallel flow solution which depends on both the Rayleigh number based on the horizontal temperature difference and the vertical stratification. This flow was treated both experimentally and theoretically by Elder (1965), who observed the transition from a one-dimensional flow to a sequence of two-dimensional steady flows consisting of stacked vertical convection cells which were approximately periodic in regions removed from the endwalls. Gill & Davey (1969) analysed the linear stability of the boundary layer on a heated vertical wall

† Present address: Department of Mathematics, University of Louisiana at Lafayette, LA, 70504-1010, USA.
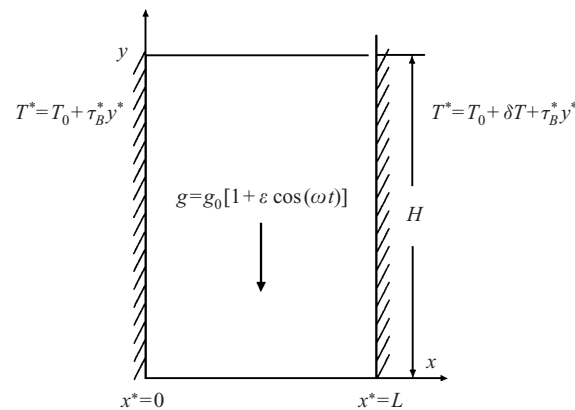
FIGURE 1. Flow geometry: the asterisk refers to dimensional quantities.

with a vertical temperature gradient at infinity – the so-called buoyancy layer. They found travelling wave and stationary modes, both of which are periodic in the axial direction. The definitive linear stability analysis was presented by Bergholz (1978) who treated the finite-width slot over a wide range of parameters, establishing the neutral curves for transition to both steady and oscillatory axially periodic modes. In recognition of these earlier seminal works, we refer to the flow under constant gravity as the Elder–Gill–Davey–Bergholz problem or EGDB flow.

As a result of these studies, there exists a fairly complete theory of the linear stability characteristics for the stratified slot, but given the size of the parameter space these results are complex in detail. Since we also consider a finite-width slot, the paper by Bergholz is the most relevant to our study. While Bergholz generally takes the Grashof number as the bifurcation parameter, we take it to be the Rayleigh number, Ra, based on the slot width and the horizontal temperature difference. With that choice, the linear stability problem is characterized by the dimensionless stratification parameter, τ_B and the Prandtl number, Pr. As discussed by both Gill & Davey and Bergholz, it is also useful to parameterize the problem by Pr, and a modified stratification parameter, γ, defined as $4\gamma^4 \overset{\text{def}}{=} \tau_B Ra$, which is the relevant parameter for large τ_B, Ra, in which the base-state flow is of a boundary layer nature. For a range of Pr, Bergholz finds both travelling and stationary axially periodic modes, which are also seen in a variety of experimental studies. He also finds the prediction of the linear theory to be in general agreement with these experimental studies, as long as the stratification parameter is estimated appropriately.

We are interested in thermal convection when time-dependent body forces are considered, as might arise in systems with density gradients subjected to vibrations, i.e. so-called g-jitter. The influence of g-jitter on thermal convection depends on the orientation of the time-dependent acceleration with respect to the thermal stratification. Much work is concerned with a vertically modulated fluid layer with constant vertical stratification, i.e. modulated Rayleigh–Bénard convection. The stability of that flow was studied by Gresho & Sani (1970). The full numerical solution for moderate and large Rayleigh numbers was provided by Biringen & Peltier (1990) where the presence of isochronous (or synchronous) and subharmonic modes of bifurcation suggested by the Galerkin truncation used by Gresho & Sani (1970) were confirmed. Analogous phenomena occur in the case of oscillatory horizontal oscillations for a laterally heated cavity, Lizée & Alexander (1997), in which case the jitter interacts

with the horizontal stratification, producing the potential for a dynamic instability of the Rayleigh–Bénard type. They find a sequence of period-doubling bifurcations as the jitter amplitude is varied, leading to aperiodic regimes at large amplitudes.

Recently, Chen & Chen (1999) considered a problem very closely related to ours, i.e. a horizontally stratified slot, but in the absence of any vertical stratification, and they focus entirely on linear instabilities. The primary difference between the problems is that the horizontally stratified slot problem has an exact parallel flow solution, *with no potential for parametric instability*. Their unmodulated problem has linear instability modes that are either shear or buoyancy driven, depending on the value of Pr, and their main focus is on the effect of jitter on the critical conditions for onset of axially periodic two-dimensional convection. They report the onset of isochronous, subharmonic, and quasi-periodic modes, depending on the axial wavenumber, and find that jitter can either stabilize or destabilize the slot, depending on the amplitude and frequency, but that jitter does not change the physical mechanism of instability.

In the case of the stratified slot under consideration here, we can anticipate three classes of effects associated with jitter. First, the interaction of the jitter with the flow produced by the steady component of gravity may lead to parametric instability, as first studied by Farooq & Homsy (1996). Second, when the parameters are such that travelling waves are the normal modes for the unmodulated case, we anticipate resonant interaction with the jitter when the frequencies are commensurate and the parameters are such that the system is near the neutral curve of the EGDB problem. Finally, when stationary modes (standing waves) are the relevant mode of instability, we are interested in the possibility that the jitter can modify the parameters so as to produce a mixed mode of both travelling and stationary waves.

Our work is also motivated by the findings of Farooq & Homsy (1996). They established that the vertically stratified slot with jitter admitted parallel flow solutions. For weak jitter, they found resonances with the natural modes of the unmodulated problem. Perhaps more interestingly, they treated the problem of parametric instability for the case of large jitter amplitude by developing approximate stability maps based on a Galerkin expansion of the Boussinesq equations. Their results covered only a narrow range of Pr and γ, but showed results characteristic of the stability chart for Mathieu-type equations. They then studied the flow above the parametric stability limit by a two-term Galerkin expansion of the two-dimensional flow, resulting in a nonlinear dynamical system. Numerical studies of this system yielded complex time-dependence, including high-frequency, short-duration intermittent turbulent bursts in the response of the two-dimensional secondary flow. One of the motivations of the current work is to examine whether or not the complex time behaviour exhibited by the dynamical system is characteristic of the solutions of the full two-dimensional partial differential equations.

Having established the main objectives of the paper, we now discuss our choices of parameters in more detail. As mentioned above, the dimension of the parameter space for the jitter problem is large. In addition to those parameters characterizing the EGDB flow (Ra, Pr, γ), the jitter problem involves the dimensionless jitter amplitude, ϵ, and frequency, ω, making this a five-dimensional problem. Obviously a complete parametric study is out of the question, so we confine our study to regions of parameter space where more narrowly focused questions may be answered unequivocally. As mentioned above, we take Ra as the bifurcation parameter for the steady EGDB problem, while for the jitter problem, we take it to be the jitter amplitude, ϵ. We treat the Prandtl number range $Pr = 0.73$ to $Pr = 10^3$ for the parametric resonance studies, and more restricted set of values for the other studies.

We give the following overview of the range of our studies. For the case of constant gravity (EGDB problem), we solve the full nonlinear Boussinesq equations for large Prandtl number, $Pr = 1000$. As will be seen, the different modes found by Bergholz (1978) are well separated in terms of the stratification parameter γ. Accordingly, our work on the EGDB problem focused on the following specific points:

(i) a study for $Ra = 3 \times 10^5$ for four different $\gamma = 2, 6, 8, 10$ in which we recover the three different regimes as predicted by linear theory (Bergholz 1978);

(ii) a study of cases for which more than one mode is linearly unstable in order to determine which mode is selected by the full nonlinear equations;

(iii) an investigation of the presence or absence of subcritical or secondary bifurcation.

For the case with gravity modulation we:

(i) obtain accurate stability maps for the parametric instability of the plane-parallel one-dimensional flow for several Pr, extending and improving the results in Farooq & Homsy (1996);

(ii) identify the mechanism for the parametric instability and its dependence on Pr, γ through the derivation and analysis of a generalized energy evolution equation;

(iii) interrogate the dynamics of the flow for a variety of parameters for both sub- and super-critical jitter amplitudes ϵ;

(iv) examine the extent to which the numerical solutions of the full equations mimic the behaviour of the truncated Galerkin expansion of Farooq & Homsy (1996).

The outline of the paper is as follows. Following a brief statement of the basic equations, scalings, and the operator-splitting finite difference scheme, we first solve the nonlinear EGDB problem in regions of parameter space in which multiple modes are simultaneously unstable, focusing on the case $Pr = 10^3$. We then go on to a detailed study of the stability maps for the jitter case for a range of Pr for fixed Ra and γ. Having established the stability maps and discussed the mechanism, we then conduct simulations above the critical jitter amplitude to determine the evolution of the flow in two dimensions.

2. Governing equations

Consider the flow in a vertical slot with a linear vertical temperature gradient and differentially heated walls, as shown in figure 1. The following dimensionless variables are introduced:

$$x = \frac{x^*}{L}, \quad y = \frac{y^*}{L}, \quad \omega = \omega^* \frac{L^2}{\kappa}, \quad t = t^* \frac{\kappa}{L^2}, \quad \psi = \frac{\psi^*}{v}, \quad \theta = \frac{T^*}{\delta T} - \frac{1}{2} - \tau_B y, \quad \tau_B = \frac{\tau_B^* L}{\delta T}.$$

The notation is standard: v is the kinematic viscosity, κ the thermal diffusivity, L the width of the slot, and δT the horizontal temperature difference, and quantities without an asterisk are dimensionless. Note that the field $\theta(x, y, t)$ is the departure from a linear vertical stratification. In accord with experimental observations and linear theory for the non-modulated case, we seek solutions which are periodic in the vertical direction with dimensionless wavelength H.

The boundary value problem under consideration then takes the form

$$\frac{1}{Pr} \frac{\partial \Delta \psi}{\partial t} + \frac{1}{Pr} \left(\frac{\partial \psi}{\partial y} \frac{\partial \Delta \psi}{\partial x} - \frac{\partial \psi}{\partial x} \frac{\partial \Delta \psi}{\partial y} \right) = -Ra \frac{\partial \theta}{\partial x} [1 + \epsilon \cos(\omega t)] + \Delta^2 \psi, \qquad (2.1)$$

$$\frac{\partial \theta}{\partial t} + \left(\frac{\partial \psi}{\partial y} \frac{\partial \theta}{\partial x} - \frac{\partial \psi}{\partial x} \frac{\partial \theta}{\partial y} \right) - \tau_B \frac{\partial \psi}{\partial x} = \Delta \theta, \qquad (2.2)$$

with boundary conditions

$$\psi = \frac{\partial \psi}{\partial x} = 0, \quad \theta = \tfrac{1}{2} \qquad \text{for} \quad x = 0, \tag{2.3}$$

$$\psi = \frac{\partial \psi}{\partial x} = 0, \quad \theta = -\tfrac{1}{2} \qquad \text{for} \quad x = 1, \tag{2.4}$$

and periodic conditions in the vertical direction

$$\left. \begin{aligned}
\psi(x,0,t) &= \psi(x,H,t), \\
\psi_y(x,0,t) &= \psi_y(x,H,t), \\
\psi_{yy}(x,0,t) &= \psi_{yy}(x,H,t), \\
\psi_{yyy}(x,0,t) &= \psi_{yyy}(x,H,t), \\
\theta(x,0,t) &= \theta(x,H,t), \\
\theta_y(x,0,t) &= \theta_y(x,H,t).
\end{aligned} \right\} \tag{2.5}$$

Here $H = H^*/L = 2\pi/\alpha$ is the dimensionless wavelength: equivalently, α is the dimensionless vertical wavenumber of the periodic solutions. Also, ϵ is the dimensionless amplitude of the jitter, ω the dimensionless jitter frequency, τ_B the dimensionless vertical temperature gradient, and Ra, Pr and γ are defined as usual:

$$Ra = \frac{\beta g_0 \delta T L^3}{\nu \kappa}, \quad Pr = \frac{\nu}{\kappa}, \quad 4\gamma^4 = \tau_B Ra,$$

where β is the coefficient of thermal expansion of the liquid, and g_0 the mean gravity.

Under the selected boundary conditions the problem admits a plane-parallel solution of the form $\Psi(x,t), \Theta(x,t)$ for which the governing system reduces to the following:

$$\frac{1}{Pr} \frac{\partial^3 \Psi}{\partial t \partial x^2} = -Ra \frac{\partial \Theta}{\partial x}[1 + \epsilon \cos(\omega t)] + \frac{\partial^4 \Psi}{\partial x^4}, \tag{2.6}$$

$$\frac{\partial \Theta}{\partial t} - \tau_B \frac{\partial \Psi}{\partial x} = \frac{\partial^2 \Theta}{\partial x^2}, \tag{2.7}$$

with the same boundary conditions (2.3), (2.4).

3. Difference scheme and algorithm

The scheme employed in the present work is a further development of that already discussed in Christov & Ridha (1994, 1995) where its performance was tested for the case of the lid-driven cavity. Here we outline the main principles upon which it is built, i.e. operator splitting and internal time iterations. The grid lines for stream function ψ and the temperature θ are staggered in time and space:

$$\psi_{ij}^n = \psi(x = h_x[i-2], y = h_y[j-1], t = \tau[n-1]),$$

$$\theta_{ij}^{n-1/2} = \theta(x = h_x[i-1.5], y = h_y[j-0.5], t = \tau[n-1.5]),$$

where h_x, h_y are the spacings in the x- and y-directions, respectively.

Central-difference approximations are used for different differential operators which secures second-order of approximation in space. Our numerical method is built on operator splitting and internal iterations. We introduce an artificial time into the

momentum equation for the stream function (2.1), rendering it ultraparabolic:

$$\frac{\partial \psi}{\partial s} = \frac{1}{Pr}\left[\frac{\partial \Delta\psi}{\partial t} + \left(\frac{\partial \psi}{\partial y}\frac{\partial \Delta\psi}{\partial x} - \frac{\partial \psi}{\partial x}\frac{\partial \Delta\psi}{\partial y}\right)\right] - \Delta\Delta\psi + Ra\frac{\partial \theta}{\partial x}[1 + \epsilon\cos(\omega t)]. \quad (3.1)$$

Then within a given time step we employ operator splitting. We use the so-called second Douglass scheme or the 'scheme of stabilizing correction' (see e.g. Yanenko 1971 for details) whose linear part is absolutely stable even for non-commuting operators:

$$\frac{\tilde{\psi}_{ij} - \psi_{ij}^{n,k}}{2\sigma} = \left(\frac{2}{\tau}\Lambda_{xx} - \Lambda_{x^4} + \frac{1}{Pr}\omega_x^{n+1/2}\Lambda_x\right)\tilde{\psi}_{ij} + \left(\frac{2}{\tau}\Lambda_{yy} - \Lambda_{y^4} - \frac{1}{Pr}\omega_y^{n+1/2}\Lambda_y\right)\psi_{ij}^{n,k}$$

$$- \left[\frac{2}{\tau}(\Lambda_{xx} + \Lambda_{yy}) + \Lambda_{x^4} + \Lambda_{y^4} - \frac{1}{Pr}\omega_x^{n+1/2}\Lambda_x + +\frac{1}{Pr}\omega_y^{n+1/2}\Lambda_y\right]\psi_{ij}^n$$

$$- \Lambda_{x^2y^2}(\psi_{ij}^{n,k+1} + \psi_{ij}^{n,k}) + Ra[1 + \epsilon\cos(\omega t^{n+1/2})]\Lambda_x\theta_{ij}^{n+1/2}, \quad (3.2)$$

$$\frac{\psi_{ij}^{n,k+1} - \tilde{\psi}_{ij}}{2\sigma} = \left(\frac{2}{\tau}\Lambda_{yy} - \frac{1}{Pr}\Lambda_{y^4} - \frac{1}{Pr}\omega_y^{n+1/2}\Lambda_y\right)[\psi_{ij}^{n,k+1} - \psi_{ij}^{n,k}]. \quad (3.3)$$

The scheme is first order with respect to the artificial time $O(\sigma)$, while it is of second order with respect to the real (physical) time and the two space variables, i.e. the truncation errors are $O(\tau^2 + h_x^2 + h_y^2)$.

In (3.3) the following notation is used:

$$\omega_{ij}^n \stackrel{\text{def}}{=} \frac{\psi_{i+1,j}^n + \psi_{i-1,j}^n - 2\psi_{ij}^n}{h_x^2} + \frac{\psi_{i,j+1}^n + \psi_{i,j-1}^n - 2\psi_{ij}^n}{h_y^2},$$

$$\omega_{ij}^{n+1/2} \stackrel{\text{def}}{=} \tfrac{1}{2}(\omega_{ij}^n + \omega_{ij}^{n+1}),$$

$$\omega_y^{n+1/2} \stackrel{\text{def}}{=} -\frac{1}{2h_y}(\omega_{i,j+1}^{n+1/2} - \omega_{i,j-1}^{n+1/2} + \omega_{i-1,j+1}^{n+1/2} - \omega_{i-1,j-1}^{n+1/2}),$$

$$\omega_x^{n+1/2} \stackrel{\text{def}}{=} \frac{1}{2h_x}(\omega_{i+1,j}^{n+1/2} - \omega_{i-1,j}^{n+1/2} + \omega_{i-1,j-1}^{n+1/2} - \omega_{i-1,j-1}^{n+1/2}),$$

and $\Lambda_{x^4}, \Lambda_{y^4}, \Lambda_{x^2y^2}, \Lambda_{xx}, \Lambda_{yy}, \Lambda_x, \Lambda_y, \Lambda_{xy}$ are central differences.

Correspondingly, for the temperature we take

$$\Lambda_x\theta_{ij} \stackrel{\text{def}}{=} \frac{1}{2h_x}(\theta_{i,j}^{n+1/2} - \theta_{i-1,j}^{n+1/2} + \theta_{i,j-1}^{n+1/2} - \theta_{i-1,j-1}^{n+1/2}),$$

which demonstrates that the θ-grid is staggered with respect to the ψ-grid.

The time-stepping with respect to the artificial time is terminated when the following criterion is satisfied:

$$\frac{\max|\psi^{n,k+1} - \psi^{n,k}|}{\sigma\max|\psi^{n,k+1}|} < 10^{-5}.$$

Note that since the time increment σ is typically $O(10^{-5})$, the required norm for convergence of the stream function is $O(10^{-10})$.

After the internal iterations (which represent an evolution with respect to the artificial time) converge, the scheme (3.2), (3.3) reduces to a fully implicit time step akin to the Arakawa scheme (see e.g. Arakawa & Lamb 1981). It is conservative for the advective terms and has no second-order artificial viscosity. As the initial

condition for this iterative process is close to the solution sought, the number of iterations is small. Since the initial condition is merely the solution from the previous physical time step, the number of iterations decreases with the decrease of the real-time increment. Conversely, if one chooses very large physical-time increments τ then the number of iterations (artificial time steps) needed for convergence becomes very large. The optimal performance is achieved when the number of the internal iterations is kept around 12–15 in the sense that the real-time increment τ is still large enough that the process evolves reasonably quickly. Theoretically, the most efficient choice is $\sigma = (Pr\tau)^2$ and this was confirmed by our numerical experiments.

The temperature equation is treated in an analogous manner as follows:

$$\frac{\tilde{\theta} - \theta^{n-1/2}}{\tau} = \tfrac{1}{2}(\Lambda_{xx} - u^n\Lambda_x)[\tilde{\theta} + \theta^{n-1/2}] + (\Lambda_{yy} - v^n\Lambda_y)\theta^{n-1/2}, \tag{3.4}$$

$$\frac{\theta^{n+1/2} - \tilde{\theta}}{\tau} = \tfrac{1}{2}(\Lambda_{yy} - v^n\Lambda_y)[\theta^{n+1/2} - \theta^{n-1/2}], \tag{3.5}$$

$$v_{ij}^n \stackrel{\text{def}}{=} \tfrac{1}{2h_y}(\psi_{i,j+1}^n - \psi_{i,j-1}^n + \psi_{i-1,j+1}^n - \psi_{i-1,j-1}^n),$$

$$u_{ij}^n \stackrel{\text{def}}{=} -\tfrac{1}{2h_x}(\omega_{i+1,j}^n - \psi_{i-1,j}^n + \omega_{i+1,j-1}^n - \psi_{i-1,j-1}^n).$$

The scheme is absolutely stable for a 'frozen' stream function. It has no artificial diffusion, because of the conservative approximation of the advective terms.

The computations in this paper were done on a variety of finite difference grids, ranging from 40×40 to 320×320. The majority of the computations were performed on a 160×160 grid, with spot checks for convergence using the finest grid. These checks show that our results on the 160×160 grid are accurate to within 1%.

Now consider the one-dimensional problem for the parallel flows. The scheme we used to solve (2.6), (2.7) is built upon the same general ideas as the scheme for the two-dimensional problem. We use the same staggered mesh:

$$\Psi_i^n = \Psi(x = h_x[i-2], t = \tau[n-1]), \quad \Theta_i^{n-1/2} = 7\Theta(x = h_x[i-1.5], t = \tau[n-1.5]),$$

and central-differences approximations of the spatial operators:

$$\frac{\Psi_{xx}^{n+1} - \Psi_{xx}^n}{\tau Pr} = \tfrac{1}{2}\Psi_{xxxx}^{n+1} + \tfrac{1}{2}\Psi_{xxxx}^n - Ra[1 + \epsilon\cos(\omega t)]\Theta_x^{n+1/2}, \tag{3.6}$$

$$\frac{\Theta^{n+3/2} - \Theta^{n+1/2}}{\tau} = \tfrac{1}{2}\Theta_{xx}^{n+1/2} + \tfrac{1}{2}\Theta_{xx}^{n-1/2} + \tau_B\Psi_x^{n+1}, \tag{3.7}$$

where h and τ are the spacing and the time increment, and the following notation is used:

$$\Psi_{xxxx}^n \stackrel{\text{def}}{=} \frac{1}{h_x^4}[\Psi_{i+2}^n - 4\Psi_{i+1}^n + 6\Psi_i^n - 4\Psi_{i-1}^n + \Psi_{i-2}^n],$$

$$\Psi_{xx}^n \stackrel{\text{def}}{=} \frac{1}{h_x^2}[\Psi_{i+1}^n - 2\Psi_i^n + \Psi_{i-1}^n], \quad \Psi_x^n \stackrel{\text{def}}{=} \frac{1}{h_x}[\Psi_{i+1}^n - \Psi_i^n],$$

$$\Theta_{xx}^{n+\frac{1}{2}} \stackrel{\text{def}}{=} \frac{1}{h_x^2}[\Theta_{i+1}^{n+\frac{1}{2}} - 2\Theta_i^{n+\frac{1}{2}} + \Theta_{i-1}^{n+\frac{1}{2}}], \quad \Theta_x^{n+\frac{1}{2}} \stackrel{\text{def}}{=} \frac{1}{h_x}[\Theta_i^{n+\frac{1}{2}} - 2\Theta_{i-1}^{n+\frac{1}{2}}].$$

As before, the scheme is fully implicit and is second order in both time and space. Calculations begin from a given initial condition $\Psi^0, \Theta^{1/2}$ and are continued
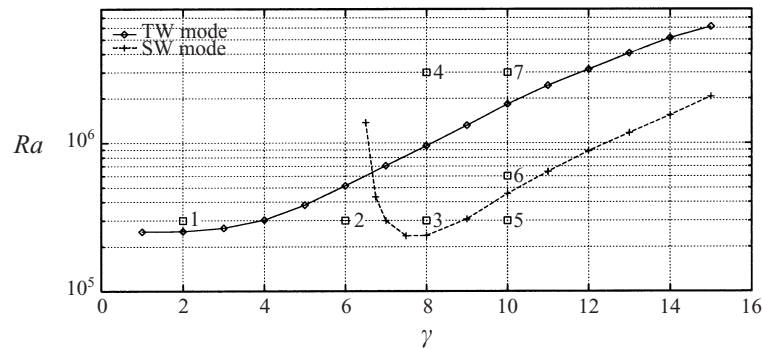
FIGURE 2. The neutral curves of Bergholz: Ra vs. γ for $Pr = 1000$. Cases treated numerically:
(1) $\gamma = 2$, $Ra = 3 \times 10^5$; (2) $\gamma = 6$, $Ra = 3 \times 10^5$; (3) $\gamma = 8$, $Ra = 3 \times 10^5$; (4) $\gamma = 8$, $Ra = 2 \times 10^6$;
(5) $\gamma = 10$, $Ra = 3 \times 10^5$; (6) $\gamma = 10$, $Ra = 6 \times 10^5$; (7) $\gamma = 10$, $Ra = 2 \times 10^6$.

until convergence in the periodic sense is reached in the stable cases or exponential divergence is observed for the unstable cases.

4. EGDB flow for $Pr = 10^3$

We first investigate the flow with constant gravity, $\epsilon = 0$. Our purpose is to validate the code, investigate the competition and interaction between travelling-wave (TW) and standing-wave (SW) modes, and, to a lesser extent, make observations regarding the possibility of subcritical or secondary bifurcations. For this, we focus on the case of high Prandtl number $Pr = 10^3$, for which the modes are fairly distinct. We consider four different values of γ. The rationale for selecting these is illustrated in the neutral curve shown in figure 2 adapted from Bergholz (1978). Extensive checks of it were conducted with the numerical code using small initial data (10^{-8}). The results of these direct numerical experiments agreed with the neutral curves shown in the figure are accurate to within a few percent. The solid line is the neutral curve for the TW solutions, the dashed curve that for the SW solutions. The cases denoted 1, 2, 3 and 5 are for the same Rayleigh number $Ra = 3 \times 10^5$ and were used primarily to validate the code. For $\gamma = 2$, $Ra = 3 \times 10^5$ (denoted by number 1) only TW solutions are expected according to the linear theory of Bergholz (1978). For $\gamma = 6$ and 10, $Ra = 3 \times 10^5$ (cases 2 and 5) no linear instability exists, while for $\gamma = 8$, $Ra = 3 \times 10^5$ (case 3) only SW solutions are expected. We also consider $\gamma = 8, 10$, $Ra = 3 \times 10^6$ (cases 4 and 7 in the figure) for which linear theory predicts coexistence of both unstable modes.

The wavenumber α is taken to be that corresponding to linear theory (Bergholz 1978), the expectation being that the wavenumber does not depend strongly on Ra for weakly supercritical conditions. In what follows, we use the symbol Ω to denote the dimensionless frequency of a particular TW mode, reserving the symbol ω for the jitter frequency. And we recall that all frequencies are made dimensionless with respect to the characteristic thermal diffusion time. The frequency of the traveling modes predicted by Bergholz can be calculated from the data for the phase speed given in figure 8 of Bergholz (1978) as $\Omega_b = c\alpha$, where the subscript denotes dimensionless quantities in the scaling used by him. Accounting for the differences in scaling between Bergholz and that used here, the dimensionless frequency of the present work (Ω_p, say) should be compared to the value $\Omega_b Ra$.
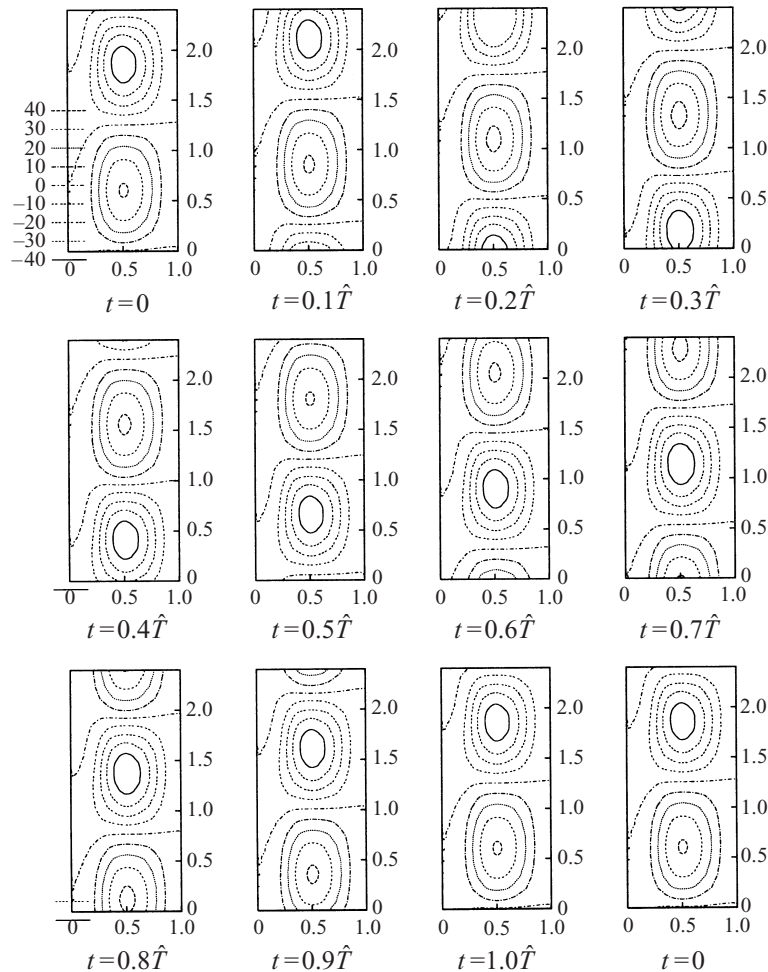
FIGURE 3. The perturbation stream lines for $Pr = 1000$, $\gamma = 2$, $Ra = 3 \times 10^5$ ($Gr = 3.10^2$), 80×80, over one period.

We begin with the Rayleigh number $Ra = 3 \times 10^5$ ($Gr = 3 \times 10^2$), $\gamma = 2$, case 1 in figure 2, for which the one-dimensional solution is unstable to a TW. We take the wavenumber from Bergholz (1978) to be $\alpha \approx 2.55$ ($H \approx 2.4$). TW solutions were obtained for three different finite difference grids: 40×40, 80×80 and 160×160. Figure 3 shows the perturbation stream function with the mean flow subtracted and with the time rescaled by multiples of the numerically determined period, $\hat{T}$. (We repeat the figure for $t = 0$ next to that for $t = \hat{T}$ so that the periodicity of the mode is made clear.) It is clear that the perturbation flow is periodic in both time and space.

The results are in very good quantitative agreement for the three resolutions. In addition, the dimensionless frequency obtained with the 40×40 grid is $\Omega = \Omega_1 \approx 5450$, that with 80×80 is $\Omega = \Omega_2 \approx 6000$, and for 160×160, $\Omega_3 \approx 6161$. A Richardson extrapolation for Ω based on the assumption that the error is $O(h^2)$ gives

$$\Omega_* = (4\Omega_2 - \Omega_1)/3 \approx 6183.$$

For the same case, the critical frequency from Bergholz (1978) is estimated to be $\Omega_b Ra \approx 6120$, which is in excellent agreement with the present results.
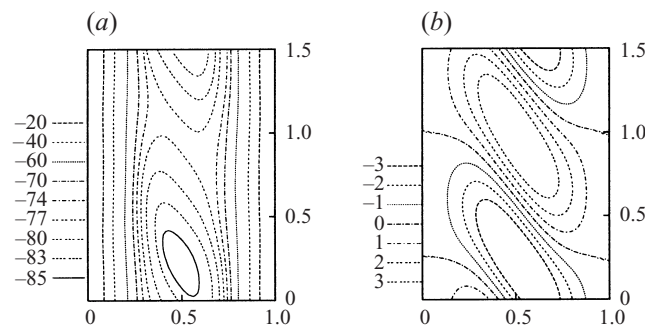
FIGURE 4. (*a*) The stream function and (*b*) its perturbation for $Pr = 1000$, $\gamma = 8$, $Ra = 3 \times 10^5$ ($Gr = 3 \times 10^2$), 40×40, $\alpha = 4.18$, $H = 1.5$.

We next consider $\gamma = 6$, $Ra = 3 \times 10^5$. The critical wavenumber from Bergholz is $\alpha = 3.6$, ($H = 1.74$). In this case the perturbation was observed to develop extremely slowly, if at all, and attempts to nucleate a finite-amplitude solution by relaxing the error tolerance were unsuccessful. We conclude that there is no two-dimensional solution for this set of parameters, thus confirming the findings of the linear instability theory (Bergholz 1978).

We next consider $\gamma = 8$. First we obtain a numerical solution for $Ra = 3 \times 10^5$ (case 3 in figure 2) when the linear theory predicts a SW solution only. The dimensionless frequency for a 40×40 grid is $\Omega \approx 20$. Increasing the resolution to 80×80 reduces the frequency by a factor of two, $\Omega \approx 10$, and in particular, brings it closer to $\Omega = 0$. Within the expected phase error of the scheme we conclude that the results represent steady two-dimensional SW, the mode consistent with linear theory. Results are shown in figure 4. Panel (*a*) shows the full flow, and (*b*) shows the mode shape of the steady cells, i.e. the perturbation flow with the mean flow subtracted. These SW patterns, with their characteristic tilt relative to the horizontal, are in good agreement with the experiments of Elder (1965).

Next we investigate the transition from a standing-wave solution to a travelling-wave with $\gamma = 8$ and $Ra = 3 \times 10^6$, case 4 in figure 2. Results for the perturbation stream function (not shown) consist of a periodic wave with a characteristic mode shape very similar to that found for $\gamma = 2$ shown in figure 3.

We consider the largest value of $\gamma = 10$ and begin with $Ra = 3 \times 10^5$ (case 5). Starting from a reasonably small initial perturbation, or with the steady solution for $\gamma = 8$, only a trivial solution is obtained, which is again in agreement with linear theory.

According to Bergholz (1978), non-trivial two-dimensional flows should exist for larger Rayleigh number, say, $Ra = 6 \times 10^5$ (case 6 in figure 2). Once again the result for the SW from the previous subsection is used as an initial condition. According to figure 7 of Bergholz (1978) the most dangerous wavelength is $\alpha = 4.6$, ($H = 1.4$). As before, a slow drift of the solution is observed. The computed frequency of the oscillations is very small: $\Omega = 22.8$ for the 40×40 grid and $\Omega = 11.35$ for 80×80. Thus the same tendency is observed as in the previous case, i.e. a nearly steady solution, in which doubling the resolution resulted in a twofold decrease in the frequency, and we again conclude that within the expected phase error of the scheme the results obtained here are steady SW modes. The patterns associated with SW modes (not shown) are very similar to those in figure 4 and are in good agreement with the experiments of Elder (1965).

Finally we proceed to $Ra = 3 \times 10^6$ (case 7 in figure 2) with the solution for $Ra = 6 \times 10^5$ taken as an initial condition. The flow quickly transforms from a SW mode to a transient solution which eventually settles down to a TW mode with frequency $\Omega = 1.5 \times 10^4$, again showing the dominance of the TW mode in the nonlinear regime.

Since our numerical scheme is fully nonlinear, we can partially address the issue of subcritical or secondary bifurcation of the EGDB flow. The transition from SW to TW modes (cases 4 and 7 in figure 2) and/or the direct transition to TW, (case 1 in figure 2), were observed to be subcritical in the sense that the TW, once established, can be sustained for values of Ra below the neutral curve, with the depth of the subcritical region estimated on the order of 5% of the critical Rayleigh number. Subcritical convection is also observed very near the neutral curve for the standing waves, but the depth of the subcritical region is much smaller than for TW. Over the range of parameters studied, subcritical bifurcation is the rule rather than the exception. There are two possibilities for this observed behaviour. Either the pure modes (TW or SW) bifurcate subcritically or there is a secondary bifurcation to a mixed mode. In either case, the region in which the convection is not dominated by a pure mode is small and of secondary interest to our study.

We can summarize our findings for the EGDB flow as follows:

(i) the features of the fully nonlinear two-dimensional solutions compare quantitatively well with the predictions of the linear instability theory with regard to mode selection, frequencies of the TW modes, and the mode shapes;

(ii) in the cases studied involving two unstable modes, the TW dominates over the SW;

(iii) the typical nonlinear feature is subcritical bifurcation, the range of which is modest for the TW modes, and very small for the SW modes.

5. One-dimensional flows with g-jitter: parametric instabilities

In this section we interrogate the one-dimensional time-dependent flow governed by equations (2.6), (2.7). The earlier study by Farooq & Homsy (1996), based on a truncated Galerkin expansion, showed that the parallel flow can undergo a parametric instability if the amplitude of the jitter is sufficiently large. Spot checks done by these authors suggested that the Galerkin results were in qualitative agreement with solutions of the full partial differential equations. Accordingly, our interest in this section is the occurrence of parametric instability for large jitter amplitudes, the corresponding stability maps, their dependence on Pr, and an identification of the mechanism of the parametric instability.

We begin with some general considerations based on two versions of generalized energy evolution equations and associated inequalities. First, as is expected, the one-dimensional flow is absolutely stable to one-dimensional disturbances for $\epsilon = 0$ (no jitter). This is obvious on physical grounds, since the steady parallel flow is an exact solution, and there are no nonlinearities that can drive instability. This result may be established mathematically through an energy inequality. The unknown function θ can be eliminated, leading to the following linear, constant-coefficient equation:

$$\frac{1}{Pr}\Psi_{ttxx} = -4\gamma^4 \Psi_{xx} - \Psi_{xxxxxx} + 2\Psi_{txxxx}, \quad 4\gamma^4 \overset{\text{def}}{=} \tau_B Ra. \quad (5.1)$$

This equation can be interpreted as a generalized wave equation containing both dispersion and dissipation. Its solutions can never diverge since the following generalized

energy estimate holds:

$$\frac{\mathrm{d}}{\mathrm{d}t} \int_0^1 \frac{1}{2} \left[\frac{1}{Pr} \Psi_{xt}^2 + 4\gamma^4 \Psi_x^2 + \Psi_{xxx}^2 \right] \mathrm{d}x = -2 \int_0^1 \Psi_{xxt}^2 \mathrm{d}x < 0. \tag{5.2}$$

Equation (5.1) is useful because one can identify regions of ω for which resonances might occur. The characteristic frequency in the non-jitter case is the Brunt–Väisälä frequency

$$N \approx 2\gamma^2 \sqrt{Pr} = \sqrt{\tau_B Ra Pr}, \tag{5.3}$$

and resonances are expected around N.

Obviously the stability result does not hold for the modulated case, in which a complicated energy-input term appears in the equation which is the counterpart of (5.1). However, the following generalized energy evolution equation can be derived in the case of modulated jitter:

$$\frac{\mathrm{d}}{\mathrm{d}t} \int_0^1 \frac{1}{2} \left[Ra\Theta^2 + \frac{\tau_B}{Pr} \Psi_x^2 \right] \mathrm{d}x$$

$$= -\tau_B \int_0^1 \Psi_{xx}^2 \mathrm{d}x - Ra \int_0^1 \Theta_x^2 \mathrm{d}x + \tau_B Ra\epsilon \cos(\omega t) \int_0^1 \Psi \Theta_x \mathrm{d}x. \tag{5.4}$$

The last term is not negative-definite: indeed, depending on the parameters and the shape of the solution it can assume sufficiently large positive values to dominate the dissipative terms and lead to instability. Equation (5.4) will be useful later in discussing the mechanism of the parametric instability and its dependence on Pr.

The stability of the one-dimensional flow is interrogated using the difference scheme (3.7) and the Floquet definition of (in)stability of time-periodic flows. For a selected value of ω the magnitude of ϵ is found for which the motion becomes divergent and therefore unstable. The calculations start from some suitably chosen initial condition and are continued until a periodic solution with a growing or decaying envelope is achieved. It turns out to be tricky to decide whether and when the solution diverges. Depending on the initial condition, in some cases the solution exhibits an increasing amplitude for as many as 200 periods and then the trend reverses to end in a stable solution after thousands of time periods. This behaviour is especially dominant near the neutral curve where the growth or damping rates are very small.

When for a given ω a value for ϵ is reached for which instability takes place, the method of interval-halving is used in order to determine the critical value of ϵ to three digits. The temporal profiles of any physical variable (velocity, temperature, etc.) at a point then determine whether the bifurcation is isochronous or subharmonic. The accuracy of the neutral curves was carefully checked by time-step refinement. In regions where the neutral curves are very steep, typically near the transition from one mode to another, a very dense set of values for ω was used, which required significant computational resources.

We first consider the case $Pr = 0.73$, $Ra = 5.1166 \times 10^5$, $\tau_B = 0.16211$ ($\gamma \approx 12$, $Gr = 7.009 \times 10^5$) which was thoroughly examined by Farooq & Homsy (1996). The stability diagram of the critical amplitude ϵ_c as a function of the jitter frequency ω is presented in figure 5. These results are seen to be in good qualitative but not quantitative agreement with figure 9 of Farooq & Homsy (1996). This is to be expected, since the latter results were based on a truncated Galerkin expansion while the present results are obtained from the partial differential equations. We find that,
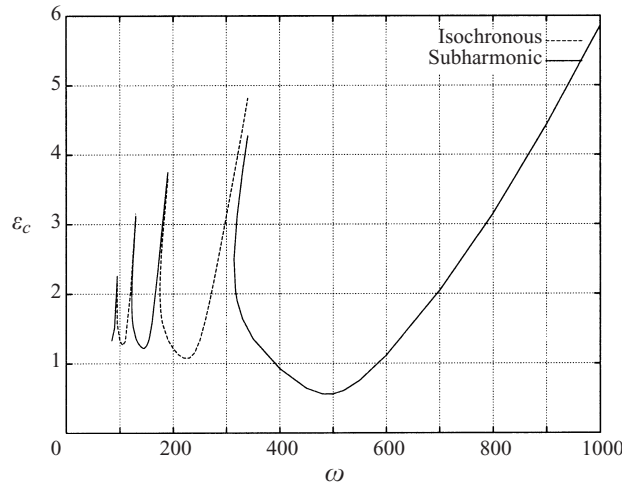
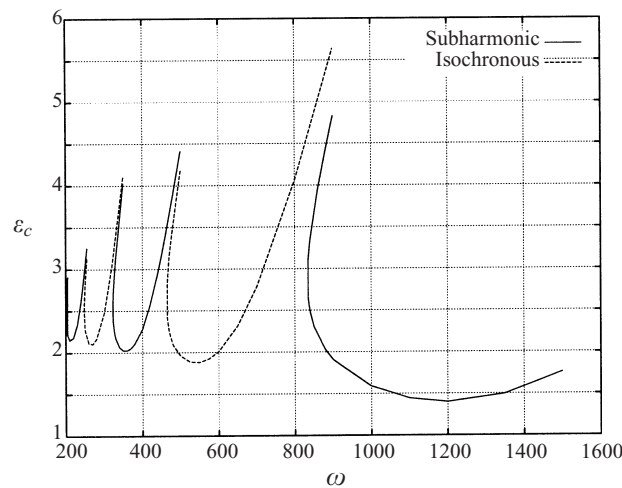FIGURE 5. $Pr = 0.73$, $Ra = 5.11650 \times 10^5$, $\tau_B = 0.16211$ ($\gamma \approx 12$, $Gr = 7.009 \times 10^5$).

FIGURE 6. $Pr = 10$, $Ra = 10^5$, $\tau_B = 0.4$ ($\gamma = 10$, $Gr = 10^4$).

as expected, either isochronous (harmonic) or subharmonic modes are observed and these are represented by solid and dashed lines, respectively.

Results for large Pr indicated both a significant change in the nature of the stability diagrams and a significant stabilization of the flow as Pr varied. In order to understand these trends we conducted a short parametric study in Pr. Figure 6 shows the results for an intermediate Prandtl number $Pr = 10$. As can be seen, the results are qualitatively the same as for $Pr = 0.73$ (figure 5). The only difference is a slight general rise in the numerical values of ϵ_c.

Figure 7 shows the results for $Pr = 100$. We note that for small ω the neutral curve is monotonically increasing, while in the intermediate range it strongly resembles the sequence of isochronous/subharmonic bifurcations that occur for $Pr = 0.73$, and $Pr = 10$. By comparing figures 6 and 7, we see a significant trend toward stabilization of the layer as Pr increases, holding Ra, γ fixed. This trend is accentuated at still higher Pr.
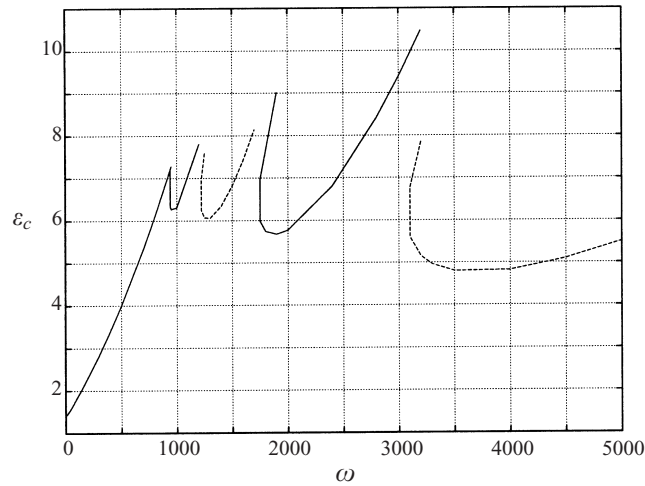
FIGURE 7. $Pr = 100$, $Ra = 10^5$, $\tau_B = 0.4$ ($\gamma = 10$, $Gr = 10^3$).
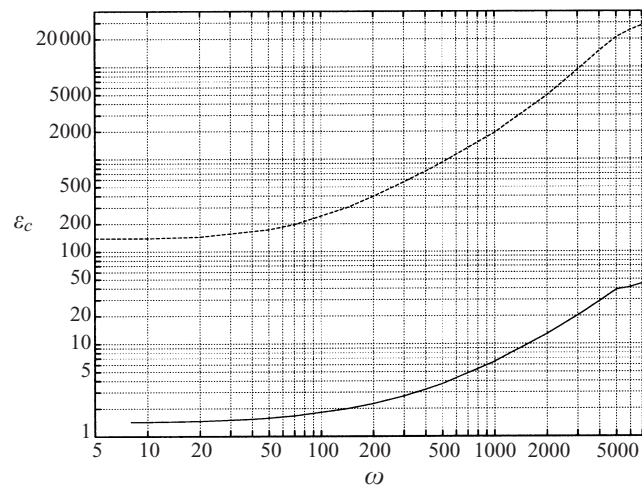
FIGURE 8. $Pr = 1000$, dashed line: $Ra = 5.0 \times 10^5$ ($Gr = 500$) $\gamma = 2$ ($\tau_B = 0.000128$); solid line: $Ra = 10^5$ ($Gr = 100$), $\gamma = 10$ ($\tau_B = 0.4$).

At very large $Pr = 1000$, the stability map changes character completely. We carried the calculations up to $\omega = 7000$ in order to cover the range of the natural frequency of the TW solution to the EGDB problem, and the results are shown in logarithmic scales in figure 8. As can be seen, we find only the isochronous mode, a monotonic neutral curve, and very significant stabilization of the flow. (Figure 8 contains results not only for $\gamma = 10$, $Ra = 10^5$ for comparison with earlier results, but also $\gamma = 2$, $Ra = 5 \times 10^5$, which is relevant to studies in a later section.) The flow is found to be less stable for the larger γ, in general agreement with the results of Farooq & Homsy (1996).

We wish to understand the dramatic differences in the stability maps for small and large Prandtl numbers. The first qualitative difference is that there are several branches of isochronous and subharmonic bifurcations for moderate Pr while only the isochronous branch is extant for $Pr = 1000$. We shall not dwell on this point

because additional branches could appear for extremely large frequencies ω for $Pr = 1000$, which if they exist, would be at very large ϵ. The second difference is that the critical jitter amplitudes increase dramatically with Pr. This can be attributed to the interplay of the fluid and thermal inertia and helps us understand the mechanism responsible for the parametric resonance. Indeed, the energy balance (5.4) asserts that the instability can occur only when the last term in the right-hand side is sufficiently large to overcome the dissipation. It is evident that this can only happen when the velocity and thermal fields, Ψ and Θ, are in temporal phase with one another. The stabilization observed for large Pr is symptomatic of the fact that they are in anti-phase, while for small to moderate Pr these two functions become more synchronized. This fact can be inferred easily from the basic equations, (2.6), (2.7). Equation (2.7) indicates that vertical stratification forces the temperature field to be out of phase with the corresponding harmonic component of the stream function. Now for large Pr, equation (2.6) indicates that in the absence of fluid inertia, the flow is in quasi-static balance with the buoyancy and it is easy to understand the lack of a temporal phase shift between the flow and temperature fields, since there is only weak coupling between the harmonics, and then only for large ϵ. For moderate Pr however, finite fluid inertia breaks the quasi-static balance, producing a phase lag between the buoyancy and the fluid response, leading to in-phase components of temperature and flow at moderate ε. This makes clear the fact that fluid inertia is the primary mechanism of the parametric instability. This interpretation was latent in the oscillator equation derived by Farooq & Homsy (1996 equation (25)), but because of the scaling used, it was neither obvious nor exploited by them. Equation (5.4) also makes clear the role of γ rather than τ_B in determining the stability, as it is the product $\tau_B Ra$ that measures the magnitude of the destabilizing term. Finally, it is clear from this energy balance that the layer is destabilized by larger vertical stratification γ, as seen in figure 8, since both the jitter amplitude and the stratification multiply the destabilizing term.

Thus our main conclusions from this section are:

(i) the features observed by Farooq & Homsy (1996) based on a Galerkin expansion are consistent with the solutions of the partial differential equations, but are quantitatively different;

(ii) the modulated, stratified slot always undergoes a parametric instability to either harmonic or subharmonic modes at a critical jitter amplitude, which increases with increasing Pr;

(iii) the mechanism of the instability is inertial in origin, and relies on an inertially induced phase lag between the velocity and temperature fields.

6. Two-dimensional flows with jitter

In this section, we study the interaction of jitter with two-dimensional solutions, both above and below the neutral curves that have been generated in the previous section. We are particularly interested in understanding the flow that replaces the linearly unstable one-dimensional flow, the important mechanisms of interaction between the jitter and the vertical stratification, and possible resonances between the jitter and two-dimensional instability modes. We are also interested in the degree to which the results of the dynamical system approximation to the two-dimensional problem discussed by Farooq & Homsy (1996) are representative of the solutions to the partial differential equations.
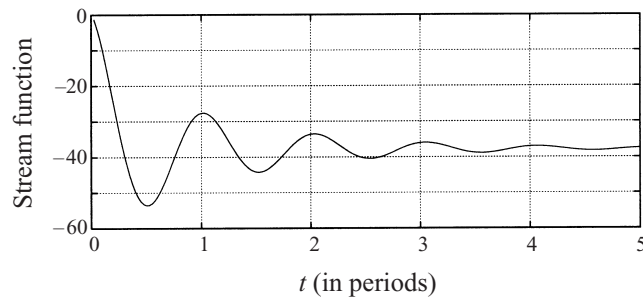
FIGURE 9. Temporal evolution of the stream function in two points for $Pr = 0.73$, $Ra = 511\,657$, $\gamma = 12$ (——, $y = 0$; – – –, $y = \pi$). Note that they overlap.

6.1. *Moderate Pr*

We begin with *case I* of Farooq & Homsy (1996): $Pr = 0.73, Ra = 511657, \gamma = 12$, which was chosen by them because the instability mode is an internal wave and the least-damped mode is a long wave. We first conducted numerical simulations for the unmodulated case to establish the dynamics without jitter. The linear-stability results of Bergholz (1978) indicate that for this case no two-dimensional linear instabilities are present, but these conditions are very near the neutral curve for the onset of TW modes. We take $H = 1.8$ which corresponds to wavenumber $\alpha \approx 3.52$ and create initial conditions containing large-amplitude localized perturbations with opposite signs located at vertical positions $\frac{1}{4}$ and $\frac{3}{4}$ of the periodic unit cell. In this way our initial conditions contain all the different harmonics, including the long-wave mode, $\alpha = 0$, with roughly equal amplitudes. The presence of this long-wave mode is significant since, from the work of Farooq & Homsy (1996), and the energy evolution equations (see equations (5.1)–(5.4)), we expect an internal gravity wave with frequency very close to the Brunt–Väisälä frequency defined above:

$$N \stackrel{\text{def}}{=} 2\gamma^2 Pr^{1/2} = \sqrt{\tau_B PrRa}.$$

For this set of parameters, $N = 246$.

In figure 9 we show the evolution of the stream function at two points along the vertical axis of the slot. Here the time variable is scaled by the value 250, thus a periodic motion with frequency close to N will appear periodic with period 1. The two curves overlap, indicating that the motion is essentially independent of y and is damped with the expected frequency. We then varied the amplitude of the initial condition, with the result that in all cases the harmonics decayed rapidly, with the remaining motion being a one-dimensional flow with oscillating amplitude (see figure 9), i.e. the least-damped mode in the two-dimensional numerical simulations is the infinitely long wave ($\alpha \to 0$).

We now discuss our results for this case with jitter. We have seen that all natural two-dimensional modes are damped, with the natural frequency of the least-damped mode being in the vicinity of 250. At the same time the stability map for the one-dimensional flow shown in figure 5 indicates that a local minimum is present around $\omega = 250$ and that at this frequency the instability is isochronous with a critical amplitude of $\epsilon_c \approx 1.333$. The aim is to understand whether the energy of the jitter can be transformed into a finite-amplitude two-dimensional state.

We conducted a large number of simulations, the primary result of which is that a two-dimensional solution of finite amplitude exists only over a range of ϵ near the neutral curve. Starting with small initial data at $\epsilon = 1.333$, we find only the unstable one-dimensional isochronous solution with an exponentially divergent envelope. Neither was it possible to onset two-dimensional motion directly from small initial data for $\epsilon < \epsilon_c = 1.333$. However, for larger initial conditions (of order 10^3) at this same value of ϵ we succeeded in exciting a two-dimensional motion. We then studied the range of ϵ over which this two-dimensional state exists. We found nonlinear equilibrated states to exist for ϵ as low as 0.5, and that these survive only up to $\epsilon = 1.4$. The manner in which we had to force these solutions (large-amplitude two-dimensional initial data) suggests that they are an isolated branch and do not bifurcate from the one-dimensional solution. For ϵ above 1.4, the two-dimensional solution cannot successfully compete with the large amplitude of the linearly unstable flow, and the solution reverts to an exponentially unstable one-dimensional flow. As will be shown later, we attribute this to the suppression of any two-dimensional flow by the interaction of the vertical stratification with the gravity modulations. Thus we find the region of existence of weakly nonlinear two-dimensional states to be relatively small, $0.5 < \epsilon < 1.40$.

The following figures illustrate some of the features of these solutions. Figure 10 shows the amplitudes of flow and temperature as a function of time over one period, but at two points in the vertical direction, for the range of ϵ over which two-dimensional states exist. The degree of mismatch between the solutions at the two axial locations may taken as the measure of the two-dimensionality of the flow. It is seen that the flow variables consist of a large contribution from the one-dimensional flow, together with smaller contributions from the two-dimensional flow, while the temperature is strongly two-dimensional. Figure 11 shows some of the details of the two-dimensional flows for different ϵ, displayed at the end of a modulation period. Panels (*a–e*) depict the two-dimensional states for both sub- and super-critical ϵ, and it is clear that the flow becomes progressively dominated by the one-dimensional mode as ϵ increases.

One of the more intriguing aspects of these solutions is revealed upon subtracting the one-dimensional flow, and exhibiting the two-dimensional flow responsible for both the stabilization of the linearly unstable flow and the supporting of the subcritical flow. Panel (*f*) shows this two-dimensional mode. An amazing feature of our results is that this mode is *virtually independent* of ϵ. *It is a robust feature of the two-dimensional flow above the point of parametric instability that is apparently independent of the parameters*. Increasing ϵ only increases the strength of the total flow, rendering the two-dimensional portion of relatively smaller magnitude. For larger ϵ, this two-dimensional mode cannot successfully compete with the linearly unstable one-dimensional flow and is completely suppressed, leading to a run-away.

We conducted similar simulations for $\omega = 500$ for which the instability of the one-dimensional flow is to a subharmonic mode, with critical value of the parameter $\epsilon_c \approx 0.56$: see figure 5. Once again, we obtained finite-amplitude two-dimensional states that persisted over a range of $0.5 < \epsilon < 0.8$. Figure 12 shows the flow structure of the two-dimensional state for $\epsilon = 0.8$. Panel (*a*) shows the full flow, while (*b*) shows the two-dimensional mode, both of which are very similar to those for $\omega = 250$. In particular, *the structure of the two-dimensional mode is nearly identical to that shown in figure* 11(*f*). Thus, our best evidence is that the two-dimensional mode that stabilizes the flow is remarkably independent of jitter frequency and of whether the base state is unstable to synchronous or subharmonic modes.
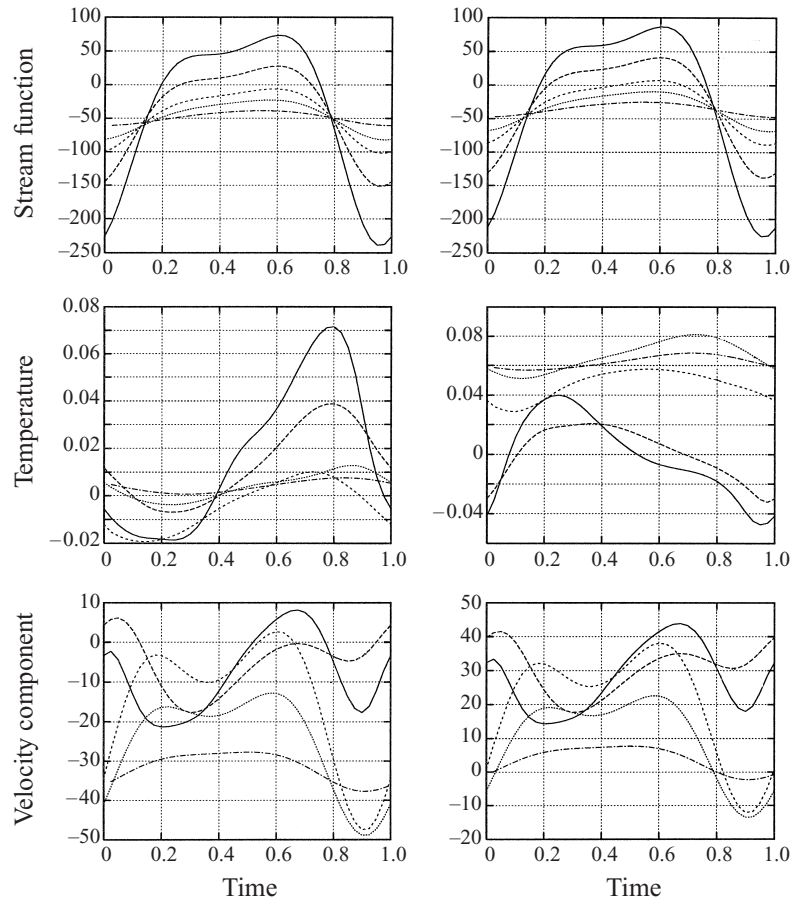
FIGURE 10. Point quantities as a function of time over one period. $Ra = 511\,650$, $Pr = 0.73$, $H = 1.8$, $x = 0.5$. The left panels present the value of the variables at $y = \pi$, while those on the right are at $y = 0$. The values of ϵ are as follows: ——, $\epsilon = 1.4$; – – –, $\epsilon = 1.333$; - - - -, $\epsilon = 1.2$; $\cdots\cdots$ $\epsilon = 1.0$; $-\cdot-\cdot-$, $\epsilon = 0.5$.

Thus, the main results of this subsection are that

(i) nonlinear two-dimensional states exist and are supported by a structure that is nearly independent of jitter amplitude, frequency, and instability mode;

(ii) the solution exhibits none of the complex time dependence that was seen in the truncated dynamical system results of Farooq & Homsy (1996);

(iii) the two-dimensional state can equilibrate the flow against strong jitter for only a narrow range of jitter amplitudes above the neutral curve.

These findings leave open the question of the flow structure at higher jitter amplitudes.

6.2. *High Pr: interaction with the TW mode*

We have seen that two-dimensional nonlinear states have difficulty surviving in competition with the linearly unstable one-dimensional flow, and we have speculated that this is due to the suppression of any two-dimensional motion due to the interaction of the jitter with the vertical stratification. In order to pursue this hypothesis further, as well as to study other parameters, we undertook a series of simulations for large
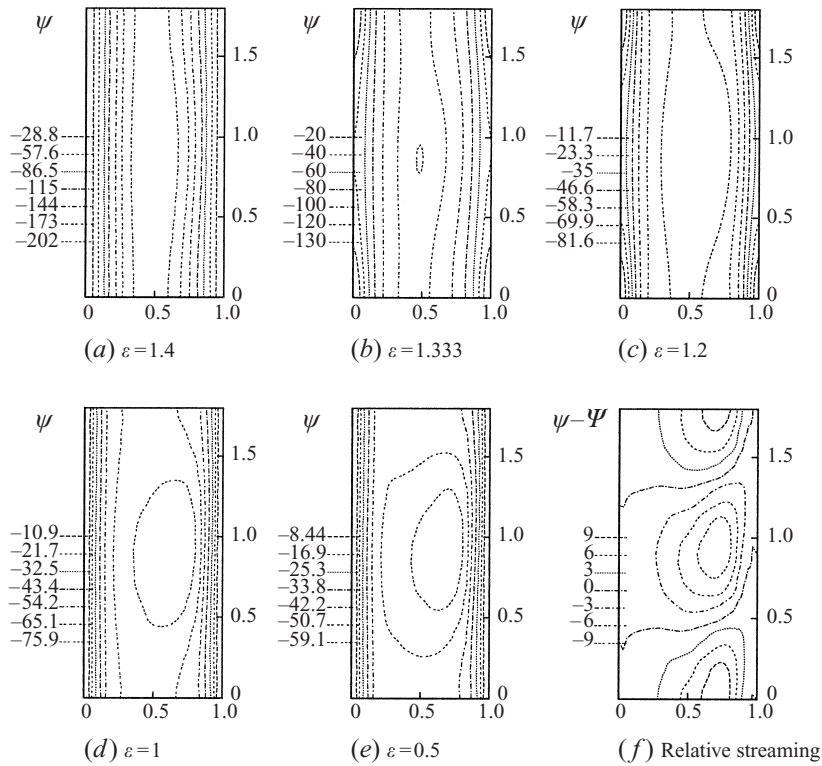
FIGURE 11. (*a–e*) The pattern of the two-dimensional flow for $Pr = 0.73$, $Ra = 5 \times 10^5$, $\gamma = 12$, $H = 1.8$, $\omega = 250$ and for different ϵ. (*f*) The perturbation of the flows in (*a–e*), which is found to be virtually independent of ϵ.
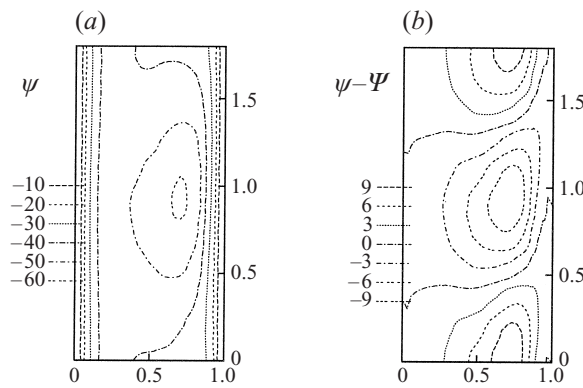

FIGURE 12. (*a*) Stream function and (*b*) relative stream function of the two-dimensional flow for $Pr = 0.73$, $Ra = 5 \times 10^5$, $\gamma = 12$, $H = 1.8$, $\omega = 500$ and $\epsilon = 0.8$.

$Pr = 1000$, for which we have established a fairly complete picture of the EGDB flow in §4.

The first case we studied was $Pr = 1000$, $Ra = 5 \times 10^5$, $\gamma = 2$. Referring to figure 2, we see that the EGDB flow is unstable to TW modes, the dimensionless frequencies of which are of order of 6000. For this range of frequencies the one-dimensional jitter flow is stable even for extremely large ϵ: see figure 8.
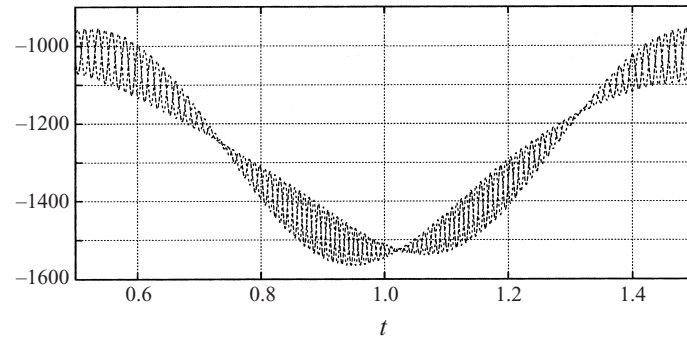
FIGURE 13. Amplitude of the stream function over one period: $Pr = 1 \times 10^3$, $Ra = 5 \times 10^5$, $\gamma = 2$, $\omega = 150$, $H = 2.8$, $\epsilon = 0.2$ (——, $y = 0$; - - - -, $y = \pi$).
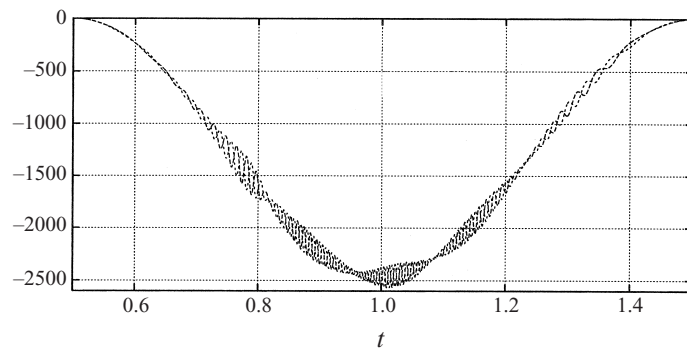

FIGURE 14. Amplitude of the stream function over one period: $Pr = 1 \times 10^3$, $Ra = 5 \times 10^5$, $\gamma = 2$, $\omega = 150$, $H = 2.8$, $\epsilon = 1.0$ (——, $y = 0$; - - - -, $y = \pi$).

We first simulated a case with small jitter amplitude at an incommensurate frequency: $\epsilon = 0.2$, $\omega = 150$. The results in figure 13, show the temporal evolution of value of the stream function at two points with different vertical coordinates both lying on the axis of the slot ($x = 0.5$; $y = \pi$ and $y = 0$), which again gives a measure of the two-dimensionality of the flow, and the time is scaled with the period of the jitter. As can clearly be seen, the response is typical of a beating pattern between the natural high-frequency Bergholz mode and the lower-frequency, one-dimensional parallel flow.

Figure 14 shows similar results, but at higher $\epsilon = 1.0$. The characteristic beating response is still present, but with a greatly reduced amplitude of the two-dimensional TW component of the solution. This is indicative of the fact that, as hypothesized above, the jitter interacts with the vertical stratification to effectively suppress two-dimensional motions. Simulations at still higher ϵ were fully consistent with these results, showing an even greater diminishing of the TW mode. Thus for these parameters, we find that even a low-frequency small-amplitude jitter stabilizes the flow against the TW modes of the EGDB problem.

Our next set of simulations examined a similar range of parameters, but for the case in which the jitter frequency was commensurate with that of the EGDB TW mode. Simulations were conducted for jitter frequencies $\omega = 5000, 6000, 7000, 8000$ which brackets the natural frequency 6200 for the set of parameters considered here. (We mention that the critical ϵ for the one-dimensional problem with $\gamma = 2$ is of

order of 20 000 for these frequencies.) Somewhat surprisingly, for $1000 \geqslant \epsilon \geqslant 100$, the flow is virtually one-dimensional, i.e. resonance phenomena were not observed for any of these frequencies, and jitter continues to suppress two-dimensional motions.

Thus the main findings of this parametric study are that there is no significant resonant interaction with TW modes of the EGDB problem, even for commensurate frequencies, and that the primary interaction between the jitter and the vertical stratification is to suppress two-dimensional motions.

6.3. *High Pr: interaction with the SW mode*

In the previous subsection we have discussed the way in which jitter interacts with the TW mode of the EGDB problem. Here we focus our attention on the interaction of jitter with the SW mode. We consider $Pr = 1000$ and focus our attention along the line $\gamma = 8$ in figure 2 where the SW modes are found, and on $Ra = 6 \times 10^5$, which places the case above the neutral curve for the SW mode. This value of Ra was selected because it also lies close to the onset of the TW mode. Thus for $\epsilon \sim O(1)$ for example, in part of the oscillation period we will have an instantaneous ('effective') Rayleigh number in the region of co-existence of both TW and SW modes, i.e. the jitter will move the instantaneous Rayleigh number above the second neutral curve in figure 2. We chose the frequency of the jitter to be $\omega = 500$, which is almost two orders of magnitude smaller than the natural frequency of the TW mode for the Rayleigh number selected, and systematically increase ϵ. Note that the bifurcation for the one-dimensional problem is to the isochronous mode with a critical value $\epsilon_c \approx 6.52$.

The temporal evolution of the stream function at two reference points $x = 0.5$, $y = 0$ and $x = 0.5, y = \pi$ is shown in figure 15 for different values of ϵ. The generic features of the solution are that as ϵ increases, jitter changes the two-dimensional stationary wave to a one-dimensional standing wave whose amplitude is synchronized with the jitter. This can be understood as follows: jitter modifies the one-dimensional flow by producing both a periodic response and a steady flow, or 'g-streaming', due to generalized inertia (Farooq & Homsy 1994). As can be seen, these one-dimensional flows can come to dominate the two-dimensional flow for large ϵ.

We find as shown in figure 15, that for $\epsilon = 1\%$, the response is around 4.5% of the mean; for $\epsilon = 10\%$, it is 13%; for $\epsilon = 50\%$, about 75%; and for $\epsilon = 110\%$, about 230%. One can see that the effect of jitter on the response scales with the magnitude of ϵ for small ϵ, but exhibits a nonlinear response for larger ϵ. The amplitude of the one-dimensional component undergoes large temporal changes (not shown in the figure) but it does not affect the circulation in the two-dimensional flow, which remains typical of the SW pattern in the absence of jitter: see e.g. figure 4. Hence the spatial pattern of the latter generally conforms to the profile of the stationary mode except for some adjustments of the amplitude analogous to increasing the Rayleigh number of the EGDB flow.

The results also indicate that for $\epsilon > 1$ the flow ceases to be strictly periodic and synchronized with the jitter. In fact for $\epsilon = 0.5$ there is a suggestion of a subharmonic bifurcation. However, it is not entirely clear that this is directly linked to the linear instability modes, since for $\epsilon = 1.1$ the solution exhibits a subharmonic mode with a frequency $\frac{2}{5}\omega$. For larger ϵ the temporal behaviour becomes even more disorganized and numerical stability of calculations is achieved only by means of a drastic reduction of the time step, making further calculations for larger ϵ problematic.

In conclusion we can say that in the range of moderate jitter amplitude, the jitter is not as effective in suppressing the SW mode as it was for the TW mode. Neither
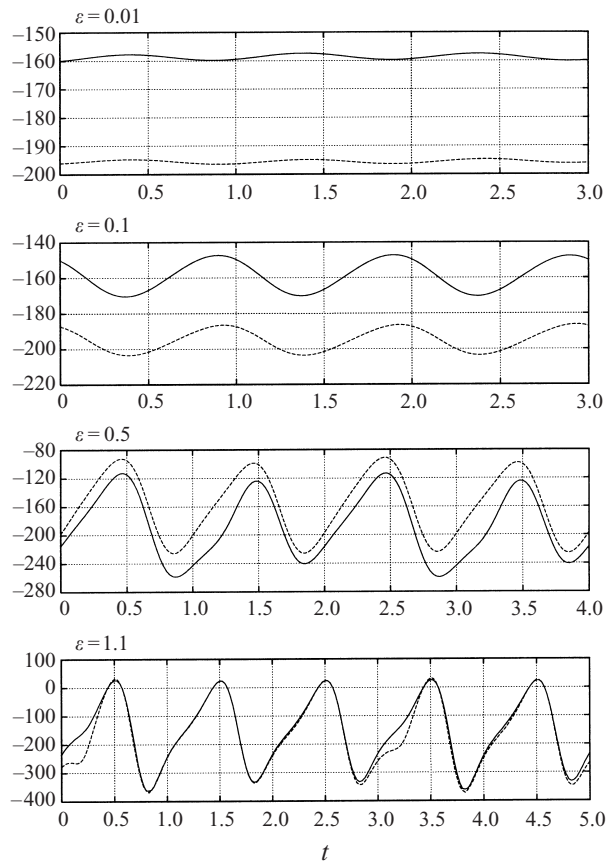
FIGURE 15. Temporal evolution (time in periods: $\bar{t} = \omega/2\pi t$) of the stream function for different ϵ and $Pr = 10^3$, $Ra = 6 \times 10^5$, $\gamma = 8$, $H = 1.74$, $\omega = 500$ ($\tau_B = 0.02731$) (——, $y = 0$; - - - -, $y = \pi$).

does it synchronize the flow to the jitter frequencies, but rather the motion becomes quasi-periodic and weakly chaotic in the sense that the temporal correlations decay on very long scales. These issues warrant an investigation that is outside the scope of the present paper.

We next consider the situation in which the jitter amplitude is increased to $\epsilon = 2.3$, holding all other parameters constant. For this choice of parameters, the jitter brings the instantaneous Rayleigh number above the transition to TW modes: see figure 2. For the steady EGDB problem, we found the dominance of the TW over SW modes when both co-exist. We are interested in the excitation of TW modes by the jitter, and whether this same dominance occurs for the time-dependent version of the problem. As mentioned above the time scale of the jitter is more than 2 orders of magnitude longer than that of the natural TW modes, which means that the jitter may appear quasi-static, and one can expect the onset of the TW modes over the first half of the jitter period.

Figure 17 shows the results, where the temporal profiles of the two selected points of the flow are juxtaposed with the (scaled) wave form of the gravity modulation. The excitation of TW modes is clearly seen in the response: indeed, in the positive part of the jitter cycle, an oscillatory mode of the frequency corresponding to that of the TW is clearly seen. On the other hand, this value $\epsilon = 2.3$ also results in a part of the jitter
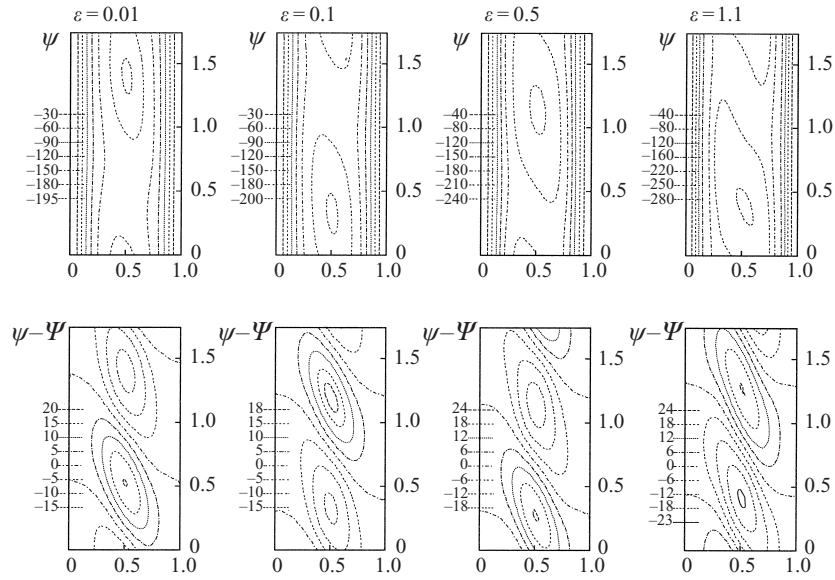
FIGURE 16. Streamline patterns for different ϵ and $Pr = 10^3$, $Ra = 6 \times 10^5$, $\gamma = 8$, $H = 1.74$, $\omega = 500$ ($\tau_B = 0.02731$). Upper panels: stream function. Lower panels: perturbation of stream function.
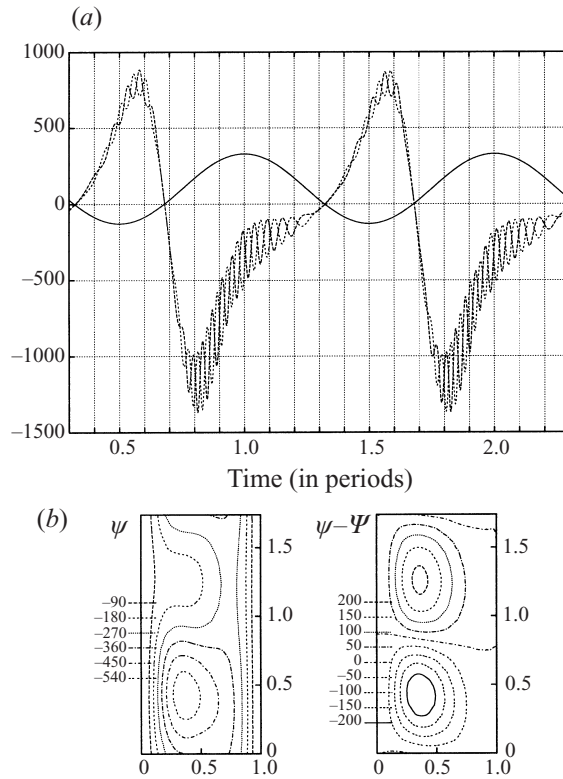

FIGURE 17. $\epsilon = 2.3$ for the case $Pr = 10^3$, $Ra = 6 \times 10^5$, $\gamma = 8$, $H = 1.74$, $\omega = 500$ ($\tau_B = 0.02731$). (a) Temporal evolution (including the gravity as a function of time) (——, $[1 + 2.3\cos(t)]$; – – –, $y = 0$; - - - -, $y = \pi$). (b) Stream function and its perturbation.
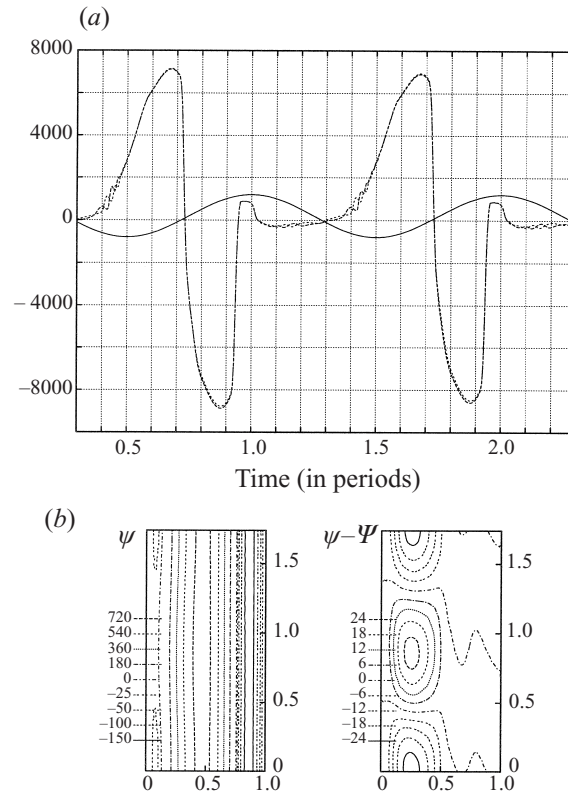
FIGURE 18. $\epsilon = 5$ for the case $Pr = 10^3$, $Ra = 6 \times 10^5$, $\gamma = 8$, $H = 1.74$, $\omega = 500$ ($\tau_B = 0.02731$). (a) Temporal evolution (including the gravity as a function of time) (——, $[1 + 5\cos(t)]$; – – –, $y = 0$; - - - -, $y = \pi$). (b) Stream function and its perturbation.

cycle for which the system is susceptible to Rayleigh–Bénard modes associated with an unstable stratification of buoyancy and a 'negative' vertical temperature gradient. Then one also expects the quasi-steady onset of Rayleigh–Bénard waves. We believe that the waves of different frequencies than the natural TW modes which are seen in figure 17(a) when $(1 + 2.3\epsilon\cos(\omega t)) < 0$ are Rayleigh–Bénard waves. Since we are witnessing the onset of TW modes (Bergholz or Rayleigh–Bénard type), it is not surprising that the spatial patterns of the flow resemble the shape of the TW normal modes, as shown in figure 17(b), which are to be compared to figure 3.

A further increase of the amplitude to $\epsilon = 5$, holding all the other parameters fixed, results in the tendency of the jitter to suppress two-dimensional modes, especially if they involve TW. Figure 18 shows the results for this value of ϵ. Over the gravitationally unstable part of the cycle, we observe weak Rayleigh–Bénard modes, but where previously we had excitation of TW modes in the stable part of the cycle, we see a suppression of the response. We believe these features are connected with the well-known stabilizing effect of acceleration, see Gresho & Sani (1970), and on the suppression of two-dimensional motion by jitter that we have discussed earlier.

In summary, this subsection has shown that the interaction of jitter with SW modes is tightly coupled, leading to an enhancement in both the steady streaming patterns and the periodic part of the response as ϵ is increased. However, the time response cannot be simply interpreted as the excitation of a subharmonic linear mode. When

the parameters are such that the instantaneous Ra is also above the transition for TW modes, these are excited as expected. However, in a scenario reminiscent of what happens in the parametric instability, the interaction of jitter with the vertical stratification suppresses the response as ϵ is increased. Finally, for larger ϵ it is possible to excite both the EGDB TW modes and unstable Rayleigh–Bénard modes over the corresponding part of the cycle.

7. Summary

In this paper we have investigated the flow and stability of a vertically stratified fluid in a finite slot both with and without gravity modulation. The problem involves a large parameter space characterized by Pr, Ra, γ (or equivalently τ_B), ϵ and ω. A complete parametric study is therefore out of the question. Accordingly, we have focused on three main issues:

(i) mode competition in the absence of jitter and for $Pr = 1000$ (for which the modes are widely separated);

(ii) the parametric instability of the parallel flow and its mechanism over a wide range of Pr;

(iii) the influence of two-dimensional flows on the parametric instability, and that of jitter on the modes which occur in the absence of jitter.

Our results for each of these topics can be summarized as follows:

(i) The nonlinear two-dimensional solutions without modulation are in general agreement with the linear stability calculations of Bergholz in the sense that the modes are well-predicted by linear theory. When both standing and travelling waves are linearly unstable, the TW dominates the SW.

(ii) Gravity modulation leads to parametric instability of the plane-parallel one-dimensional solutions. At modest Prandtl number a Floquet bifurcation to either subharmonic or isochronous modes takes place. Stability maps of critical modulation amplitude vs. modulation frequency are presented as a function of Pr. For large Prandtl number the only type of bifurcation we find is the isochronous mode. An energy equality is derived which clearly identifies the mechanism of the instability as being due to phase lags between the flow and temperature responses that are due to fluid inertia, and explains the Pr dependence of the neutral curves.

(iii) Under some conditions, two-dimensional flows replace the one-dimensional flow above the parametric instability limit. Extensive numerical experiments for $Pr = O(1)$ show nonlinear two-dimensional states for sub- and super-critical amplitudes of jitter whose temporal dependence is relatively weak. *The most remarkable feature of the solutions is the discovery of a parameter-independent two-dimensional flow structure that is responsible for stabilization of the unstable one-dimensional flow.* For highly supercritical amplitudes the plane-parallel flow diverges faster than this two-dimensional structure can stabilize it, and the flow quickly reverts to a linearly unstable one-dimensional plane-parallel motion. Thus, the region of finite-amplitude two-dimensional states is limited to the immediate vicinity of the neutral curve.

Regarding the interaction of jitter with linear instability modes of the steady EGDB problem, for large Pr, and over a range of stratification, we find that jitter of small frequency and amplitude results in a 'beating' response with high-frequency TW modes, but that this coupling is weakened as the jitter amplitude increases. Also for large Pr, but over a range of stratification for which SW are first excited, we find that the jitter produces steady streaming flows of proportionally larger amplitude. When

the jitter amplitude is sufficiently large, we find that both TW and Rayleigh–Bénard modes are excited over stable and unstable parts of the jitter cycle.

The dominant physical feature of all these flows is that gravity modulations couple *strongly* to the vertical stratification, suppressing or eliminating two-dimensional motions for stable stratification and exciting buoyancy-driven Rayleigh–Bénard modes for unstable stratification.

It remains to comment on the significant differences between the results of Farooq & Homsy (1996), which were based on severely truncated Galerkin expansions, and the present results representing accurate numerical solution of the partial differential equations. Farooq & Homsy (1996) used a two-term Galerkin expansion involving the one-dimensional flows and the least-damped two-dimensional mode. They found weakly nonlinear states above the point of parametric instability which were characterized by intermittent bursts of activity in the two-dimensional flows which stabilized the one-dimensional flow over the 'unstable' part of the cycle. In contrast, we find periodic weakly nonlinear states in which the one-dimensional flow is stabilized primarily by the robust and invariant two-dimensional flow structure alluded to above, and not by the least-damped two-dimensional linear instability mode, as assumed by Farooq & Homsy (1996). Thus the stabilization is strongly nonlinear and cannot be captured by a Galerkin expansion that does not involve the stabilizing structure as one of the trial functions.

REFERENCES

ARAKAWA, A. & LAMB, V. R. 1981 A potential enstrophy and energy conserving scheme for the shallow-water equations. *Mon. Weath. Rev.* **109**, 18–36.

BERGHOLZ, R. F. 1978 Instability of steady natural convection in a vertical fluid layer. *J. Fluid Mech.* **84**, 743–768.

BIRINGEN, S. & PELTIER, L. J. 1990 Numerical simulation of 3D Bénard convection with gravitational modulation. *Phys. Fluids* A **2**, 754–764.

CHEN, C. F. & CHEN, W.-Y. 1999 Effect of gravity modulation on the stability of convection in a vertical slot. *J. Fluid Mech.* **395**, 327–344.

CHRISTOV, C. I. & RIDHA, A. 1994 Splitting scheme for iterative solution of bi-harmonic equation. Application to 2D Navier–Stokes problems. In *Advances in Numerical Methods and Applications. Proc. 3rd Intl Conf. on Numerical Methods O(h^3) August 1994, Sofia, Bulgaria* (ed. I. Dimov, B. Sendov & P. Vasilevskii), pp. 341–352. World Scientific.

CHRISTOV, C. I. & RIDHA, A. 1995 Un schéma á pas fractionnaires de résolution de l'equation instantionnaire de fonction de courant. *C. R. Acad. Sci.* Paris **320** IIb, 441–446.

ELDER, J. W. 1965 Laminar free convection in a vertical slot. *J. Fluid Mech.* **23**, 77–98.

FAROOQ, A. & HOMSY, G. M. 1994 Streaming flows due to *g*-jitter-induced natural convection. *J. Fluid Mech.* **271**, 351–378.

FAROOQ, A. & HOMSY, G. M. 1996 Linear and nonlinear dynamics of a differentially heated slot under gravity modulation. *J. Fluid Mech.* **313**, 1–38.

GILL, A. E. & DAVERY, A. 1969 Instabilities of bouyancy-driven system. *J. Fluid Mech.* **35**, 775–798.

GRESHO, P. M. & SANI, R. L. 1970 The effects of gravity modulation on the stability of a heated fluid layer. *J. Fluid Mech.* **40**, 783–806.

LIZÉE, A. & ALEXANDER, J. 1997 Chaotic thermovibrational flow in a laterally heated cavity. *Phys. Rev.* E **56**, 4152–4156.

YANENKO, N. N. 1971 *Method of Fractional Steps*. Gordon and Breach.